Early-Life 1-Trichloromethyl-1,2,3,4-tetrahydro-betacarboline (TaClo) and 1-Methyl-4-phenyl-1,2,3,6-tetrahydropyridine (MPTP) Exposure Induces Long-Term Neurotoxicity in Adult Zebrafish (*Danio rerio*)

Ji-Hang Yin, Katharine Horzmann

Department of Pathobiology, College of Veterinary Medicine, Auburn University, Auburn, AL, USA

1 Introduction

In our previous study…

- Embryonic zebrafish served as a **good platform** for investigating the underlying mechanism of TaClo-induced neurotoxicity
- Embryonic zebrafish exposed to TaClo exhibit **neurobehavioral impairments**, **diencephalic dopaminergic neuronal damage**, **increased cellular apoptosis**, **astrocytic loss**, **microgliosis**, and **altered glutathione peroxidase (GPX) activity levels**
- 1.75 μM MPTP appeared to exhibit a **long-term neurotoxic effect** on adult zebrafish brain in both male and female

2 Purpose of study/Materials and methods

- Investigate the TaClo and MPTP induced neurotoxic effects and the underlying mechanism in **adult zebrafish brain**.
- In **Aim 3**, we evaluated the **oxidative stress** (M), **mitochondrial activity** (N), **dopaminergic neuronal expression** (O), **neurotransmitter levels** (S), and **transcriptomic alterations** (T, larvae and adult).

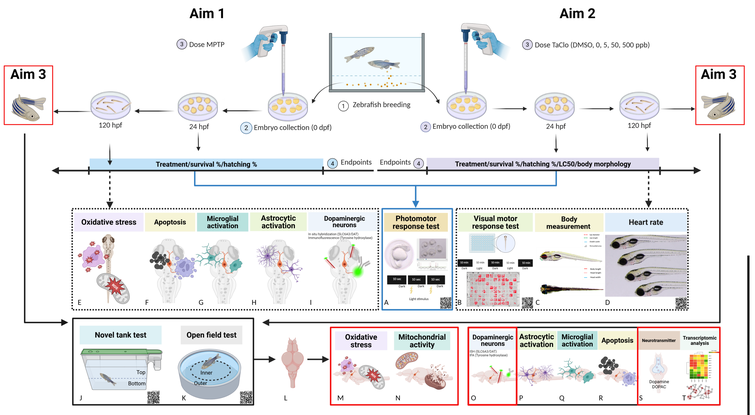

3 Results

500 ppb TaClo triggered mitochondrial oxidative stress

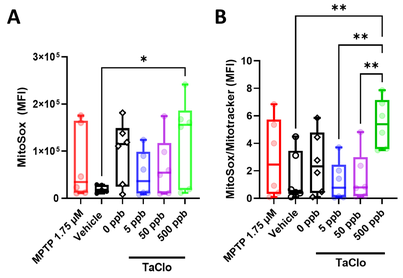

Figure 1. Oxidative stress and mitochondrial function. Single cells dissociated from treated adult zebrafish brain were subjected to flow cytometry analysis for oxidative stress and mitochondrial function. Adult zebrafish brain embryonically treated with 500 ppb TaClo had higher mitochondrial oxidative stress **(A-B)**. N=6 (1 brain per group per replicate). Error bars represent standard deviation. *,** significant difference from the vehicle (0.001% DMSO) with $p \leq 0.05$, and $p \leq 0.01$, respectively.
Auburn University Flow Cytometry and High-Speed Cell Sorting Laboratory (RRID:SCR_025507).

TaClo and MPTP (1.75 μM) exposure triggered long-term antioxidative activity responses

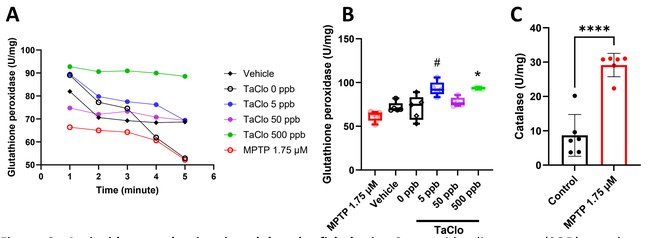

Figure 2. Antioxidant evaluation in adult zebrafish brain. Superoxide dismutase (SOD), catalase, glutathione peroxidase (GPX), and glutathione disulfide (GSSG) activity was evaluated in adult zebrafish brains. Embryonic exposure to 5 ppb **(a)** and 500 ppb **(b)** Taclo caused long-term effects with these groups having significantly higher GPX activity than all the other groups **(A-B)**. MPTP at 1.75 μM exhibited long-term effects through increased catalase activity **(C)**. Error bars represent standard deviation. **** significant difference from the vehicle (0.001% DMSO) with $p \leq 0.001$.

Early-life exposure to TaClo and MPTP led to altered neurotransmitter levels

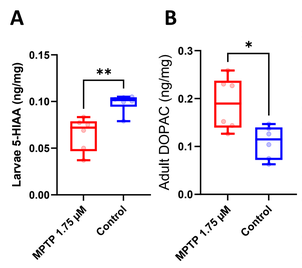

Figure 3. Neurotransmitter detection in zebrafish larvae and adult zebrafish brain. Norepinephrine, 3,4-Dihydroxyphenylacetic acid (DOPAC), dopamine, and 5-hydroxyindoleacetic acid (5-HIAA) levels were evaluated in larval zebrafish and adult zebrafish brains. Embryonic exposure to 1.75 μM MPTP resulted in significantly decreased 5-HIAA in the larvae **(A)** and significantly increased DOPAC in adult zebrafish brains **(B)** compared to the control group. Error bars represent standard deviation. ** significant difference from the control with $p \leq 0.01$. * significant difference from the control with $p \leq 0.05$.

Early-life exposure to TaClo and MPTP led to persistent diencephalic neuronal damage

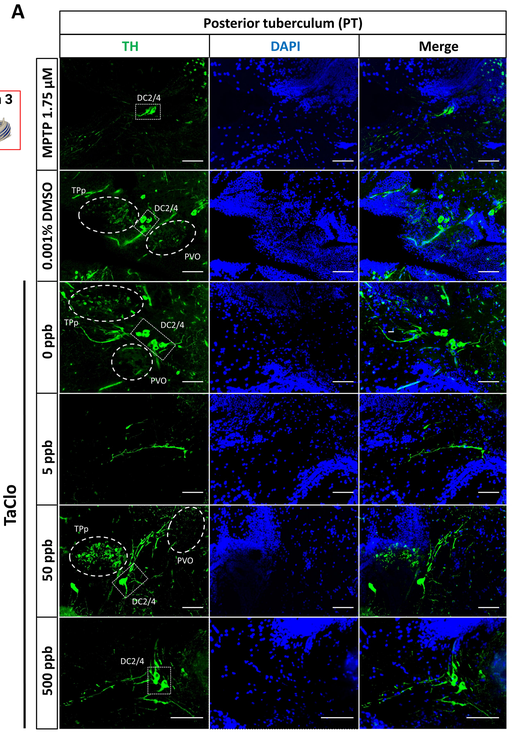

Figure 4. Images of posterior tuberculum (PT), scale bar=100 μm **(A)**. Quantitative analyses across neuronal populations at TPp **(B)**, DC2/4 **(C)**, PVO **(D)**, and PT **(E)** showed that the relative TH+ dopaminergic neuronal numbers significantly decreased in 6 mpf zebrafish with embryonic 5 ppb TaClo (5 ppb) and MPTP exposure in TPp **(B)** and DC2/4 population **(C)** compared to the control (TaClo 0 ppb) and vehicle (0.001% DMSO). Additionally, TaClo (5 ppb and 500 ppb) and MPTP treated 6 mpf zebrafish showed significantly reduced relative TH+ dopaminergic neuronal numbers in PVO **(D)** and PT **(E)** regions compared to the control and vehicle. *$p \leq 0.05$ and **$p \leq 0.001$.

Early-life exposure to TaClo inhibited stress response in larval stage

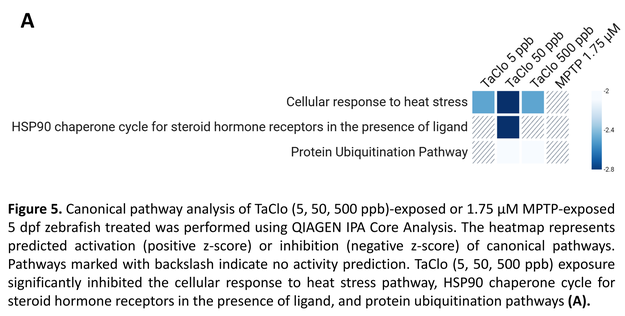

Figure 5. Canonical pathway analysis of TaClo (5, 50, 500 ppb)-exposed or 1.75 μM MPTP-exposed 5 dpf zebrafish treated was performed using QIAGEN IPA Core Analysis. The heatmap represents predicted activation (positive z-score) or inhibition (negative z-score) of canonical pathways. Pathways marked with backslash indicate no activity prediction. TaClo (5, 50, 500 ppb) exposure significantly inhibited the cellular response to heat stress pathway, HSP90 chaperone cycle for steroid hormone receptors in the presence of ligand, and protein ubiquitination pathways **(A.)**

Results

Early-life exposure to TaClo inhibited stress response in larval stage (con't)

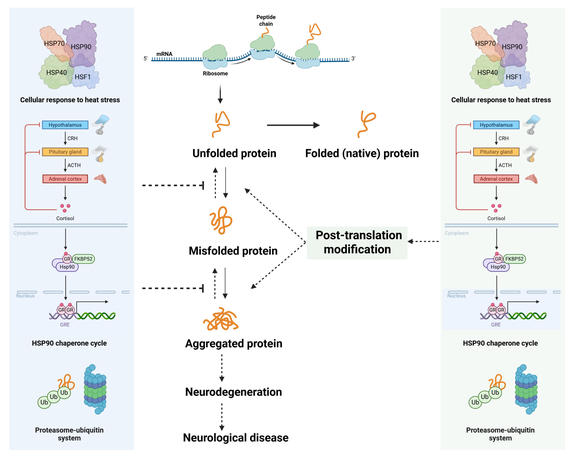

Figure 5 (Con't). TaClo exposure disrupted the larval stress response, altered post-translational modifications, and significantly affected protein folding and post-translation modification **(B)**.

500 ppb TaClo activated AHR signaling and NR2-mediated oxidative stress response in larvae

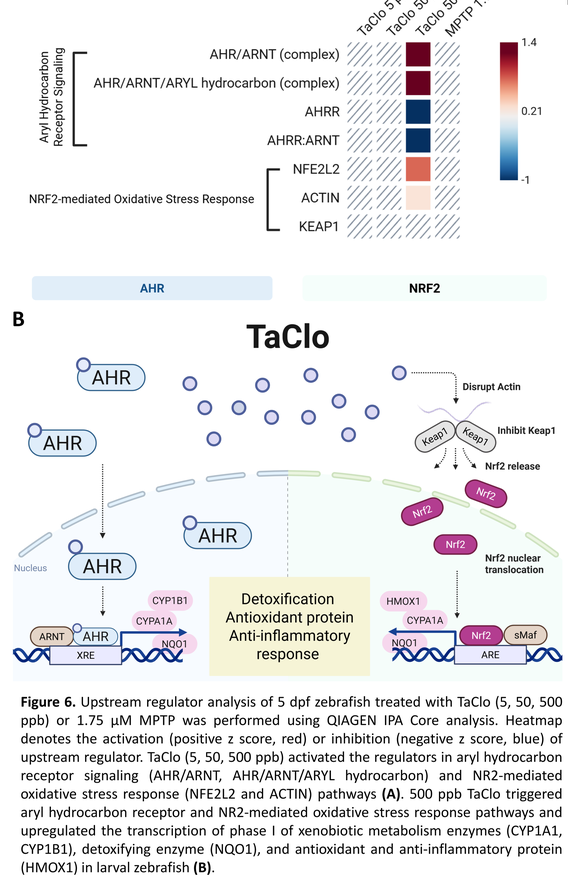

Figure 6. Upstream regulator analysis of 5 dpf zebrafish treated with TaClo (5, 50, 500 ppb) or 1.75 μM MPTP was performed using QIAGEN IPA Core analysis. Heatmap denotes the activation (positive z score, red) or inhibition (negative z score, blue) of upstream regulator. TaClo (5, 50, 500 ppb) activated the regulators in aryl hydrocarbon receptor signaling (AHR/ARNT, AHR/ARNT/ARYL hydrocarbon) and NR2-mediated oxidative stress response (NFE2L2 and ACTIN) pathways **(A)**. 500 ppb TaClo triggered aryl hydrocarbon receptor and NR2-mediated oxidative stress response pathways and upregulated the transcription of phase I of xenobiotic metabolism enzymes (CYP1A1, CYP1B1), detoxifying enzyme (NQO1), and antioxidant and anti-inflammatory protein (HMOX1) in larval zebrafish **(B)**.

1.75 μM MPTP upregulated glutamate transporter (SLCA12) expression in zebrafish larvae

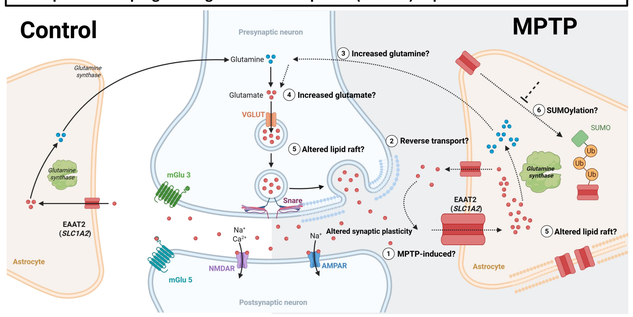

Figure 7. *SLC1A2* was significantly upregulated in larvae treated with 1.75 μM MPTP. MPTP exposure may disrupt glutamate neurotransmission at the tripartite synapse and resulted in neurological alterations in zebrafish larvae. QIAGEN IPA analysis identified activation of glutamine synthetase and metabotropic glutamate receptors (mGlu3 and mGlu5) and significantly changes in SUMOylation canonical pathway.

Early life TaClo and MPTP exposure triggered maladaptive and compensatory responses

Figure 8. In TaClo-treated larvae, an inhibited stress response with increased apoptosis and organismal death, along with decreased HSPB1 (heat shock protein beta-1) and NFKBIA (NFKB Inhibitor Alpha) expression were observed. In contrast, adult brains with early life exposure to TaClo and MPTP exhibited activation of stress-responsive canonical pathways, including serotonin receptor signaling, G-protein coupled receptor signaling, and corticotropin-releasing hormone signaling with decreased apoptosis and organismal death, along with upregulated HSPB1 and NFKBIA expression.

4 Conclusion

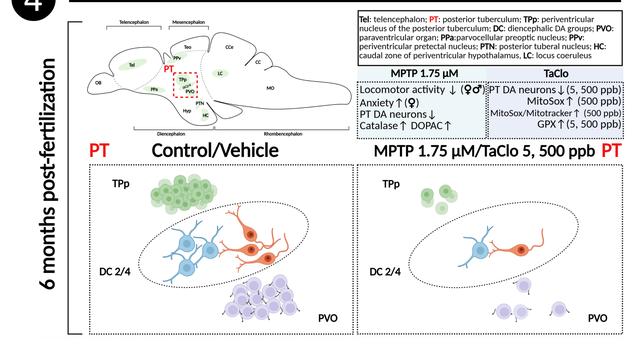

Conclusion (6 mpf):

1. Our findings demonstrate that transient ***early-life exposure*** to TaClo and MPTP leads to ***long-lasting neurotoxicity*** in adult zebrafish.
2. These results highlight the ***long-term neurotoxic risks*** of early-life TaClo and MPTP exposure and underscore the ***potential health risks*** of environmental ***TCE contamination***.

Conclusion (Transcriptomic analysis):

1. TaClo (5, 50, 500 ppb) and MPTP appear to exert neurotoxicity through **different mechanisms** during the **larval** stage by targeting at specific pathways.
2. Our results demonstrate that early exposure to TaClo (5, 50, 500 ppb) and MPTP, treated zebrafish larvae exhibit **maladaptive response** to the chemicals, while a **compensatory response** emerges in adult zebrafish brain.

Funding and Acknowledgement

- Funding: National Institute of Environmental Health Sciences R15 ES033361-01 and Auburn University College of Veterinary Medicine Animal Health and Disease Research Grant
- We thank **Dr. Rie Watanabe** for her guidance on flow cytometry (Auburn University Flow Cytometry and High-Speed Cell sorting laboratory); **Dr. Rie Watanabe , Lisa Jolly,** and **Keisha Snerling** for their guidance on cryosectioning; and **Dr. Piyush Padhi** and **Dr. Anumantha Kanthasamy** at University of Georgia for neurotransmitter detection

Severe Cerebellar Dysplasia and Congenital Hydrocephalus Associated with Mice Lacking *Hsd17b7* in *Wnt1* Cell Lineages

Bayla Bessemer[1,2], Rolf W. Stottmann[1,3]

[1] The Steve and Cindy Rasmussen Institute for Genomic Medicine, Nationwide Children's Hospital

[2]The Ohio State University College of Veterinary Medicine Department of Veterinary Biosciences

[3]The Ohio State University College of Medicine Department of Pediatrics

Nationwide Children's — When your child needs a hospital, everything matters.

The Ohio State University College of Veterinary Medicine

The Ohio State University College of Medicine

Background

Cholesterol Biosynthesis and Cholesterol in Neural Development

- Cholesterol plays an integral role in **neural development** and is involved in the formation of myelin, synapses, dendrites, and within the function of hedgehog signaling[1,2].
- Disruptions in cholesterol biosynthesis during development leads to a suite of diseases collectively referred to as **Cholesterol Biosynthesis Malformation Syndromes.** The mechanisms underlying these diseases are still poorly understood, and treatment is limited. These diseases are believed to be due not only to a decrease in cholesterol, but also an increase in potentially toxic cholesterol precursors[1,2].

Post-Squalene Biosynthesis Pathway (Simplified)

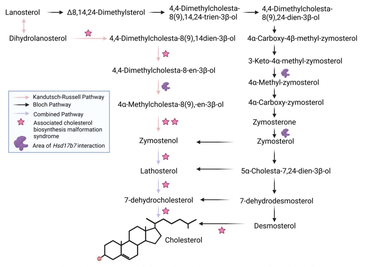

17-Beta-hydroxysteroid Dehydrogenase 7 (*Hsd17b7)* Gene

- ENU screening recovered perinatal lethal hypomorphic '*Rudolph*' mutant of *Hsd17b7*, showing that partial loss of *Hsd17b7* results in a severe CNS phenotype prompting further investigation into the role of *Hsd17b7* in organogenesis[3].

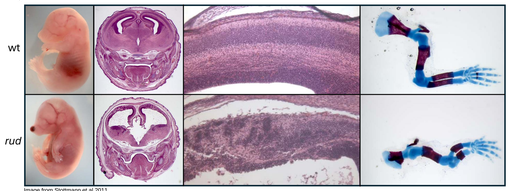

Image from Stottmann et al 2013

- Embryos at embryonic day (E)16.5 with the *Rudolph* mutation appear dysmorphic when compared to wild-type littermates. Histological analysis exposes dramatic tissue loss in the mutant as well as disrupted cortical structure and cleft palate. Mutants appear to have shortened long bones, characteristic of disturbed *Hedgehog* signaling[3].
- Tissue-specific gene ablation allows for a more in-depth understanding of the phenotypes occurring upon loss of *Hsd17b7* and their associated mechanisms.

Hypothesis/Objectives

Hypothesis: Loss of *Hsd17b7* within Wnt1 cell lineages will lead to developmental abnormalities in structures arising from the midbrain hindbrain boundary.

Objectives

- Characterize phenotypic changes in the brain associated with tissue specific ablation of *Hsd17b7* from dorsal midline
- Determine the underlying mechanisms of the noted changes

Experimental Design

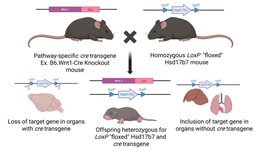

Step 1. Cre-Lox system is leveraged to delete *Hsd17b7 in Wnt-1* cell lineages, resulting in *Hsd17b7*$^{Flox/WT}$; *Wnt1cre2*$^{Cre/WT}$ mice. Genotype is confirmed through PCR. *Hsd17b7*$^{Flox/Flox}$; *Wnt1cre2*$^{Cre/WT}$ were not obtainable due to the severity of clinical disease by P17 in *Hsd17b7*$^{Flox/WT}$; *Wnt1cre2*$^{Cre/WT}$ mice.

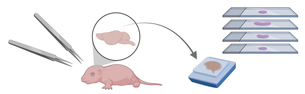

Step 2. 18 postnatal day (P)0 neonates, 33 P3 neonates, and 10 P17 mice were collected. Brains were dissected out, paraffin embedded, and were prepared for histologic examination and stained with H&E in standard fashion.

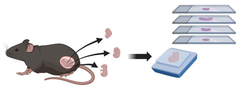

Step 3. 8 E12.5 embryos,18 E16.5 embryos, and 6 E18.5 embryos were obtained via terminal C-section, were embedded, prepared for histologic examination, and stained with H&E in standard fashion.

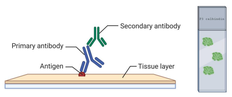

Step 4. Based on H&E findings, brains from 5 P3 mice were stained with Calbindin antibodies.

Statistical/image analysis: Minimum sample sizes were determined with *a priori* power analysis on G*Power 3.1.9.2 utilizing data from past studies. GraphPad Prism 10 was utilized to perform unpaired T-tests to determine significant differences between wildtype mice and *Hsd17b7*$^{Flox/WT}$; *Wnt1cre2*$^{Cre/WT}$ mice where necessary. A p-value of 0.05 or less was considered significant. ZEN 3.11 and NIS-elements were used for image analysis.

Hsd17b7$^{Flox/WT}$; *Wnt1cre2*$^{Cre/WT}$ mice display severe forebrain and cerebellar phenotypes

Clinical assessment, P17 Litters

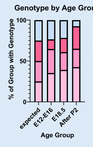

Genotyping of different age groups reveals that mutants are underrepresented at birth suggesting perinatal mortality. Mice with the pathologic phenotype must be euthanized around P17 due to the severity of neurologic signs.

Clinical assessment, P17 Litters

Hsd17b7$^{Flox/WT}$; *Wnt1cre2*$^{Cre/WT}$ mice

- Body Condition Score of 2/5 with marked muscle wasting, stunting
- Severely ataxic, slow, and frequently circled with noted intention tremors
- Severe balance deficits (flipping onto their back) with difficulty righting
- Behavior changes
  - did not run from researcher hands but generally responded to stimuli
  - Stereotypic behavior, i.e. wringing front paws

Final assessment: Mice displayed neurologic abnormalities consistent with both forebrain localization (determined to be severe hydrocephalus based on external appearance) and cerebellar localization

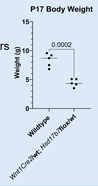

Hsd17b7$^{Flox/WT}$; *Wnt1cre2*$^{Cre/WT}$ vs WT littermates

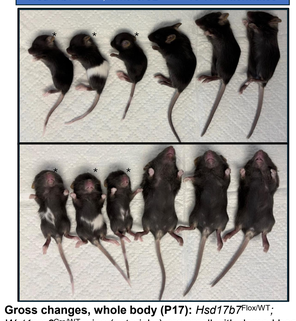

Gross changes, whole body (P17): *Hsd17b7*$^{Flox/WT}$; *Wnt1cre2*$^{Cre/WT}$ mice (asterisks) are small with domed heads and focal asymmetric white coat discoloration on midline

Wildtype | *Hsd17b7*$^{Flox/WT}$;*Wnt1cre2*$^{Cre/WT}$

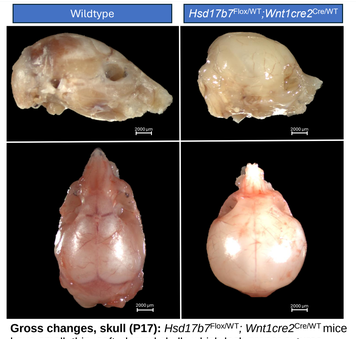

Gross changes, skull (P17): *Hsd17b7*$^{Flox/WT}$; *Wnt1cre2*$^{Cre/WT}$ mice have small, thin, soft, domed skulls which lack proper sutures between the bones of the calvaria.

Subcommissural Organ (SCO) dysplasia results in severe congenital hydrocephalus

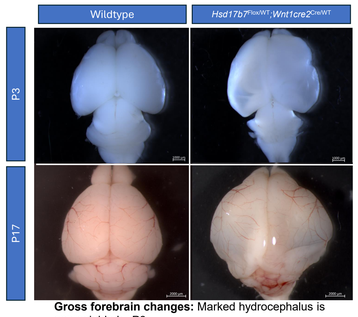

Gross forebrain changes: Marked hydrocephalus is appreciable by P3.

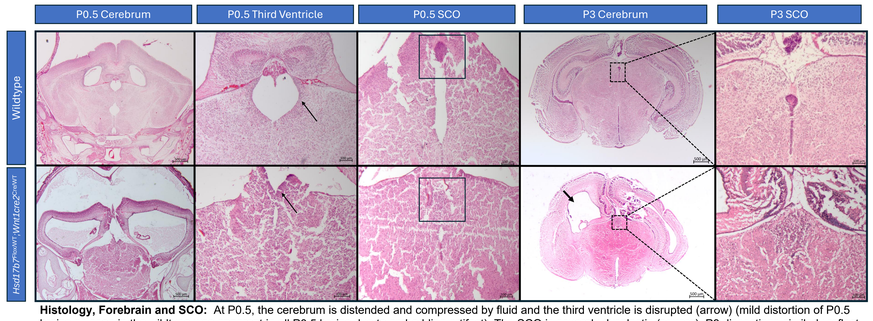

Histology, Forebrain and SCO: At P0.5, the cerebrum is distended and compressed by fluid and the third ventricle is disrupted (arrow) (mild distortion of P0.5 brains as seen in the wildtype was apparent in all P0.5 brains due to embedding artifact). The SCO is severely dysplastic (square). P3 dissections similarly reflect distension of ventricles (arrow) with a severely dysplastic SCO.

The cerebellum is hypoplastic and disorganized

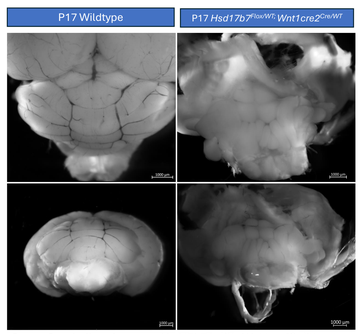

Gross Cerebellar changes: *Hsd17b7*$^{Flox/WT}$; *Wnt1cre2*$^{Cre/WT}$ cerebella are grossly small and dysmorphic with vertically oriented vermes and visible superior and inferior colliculi.

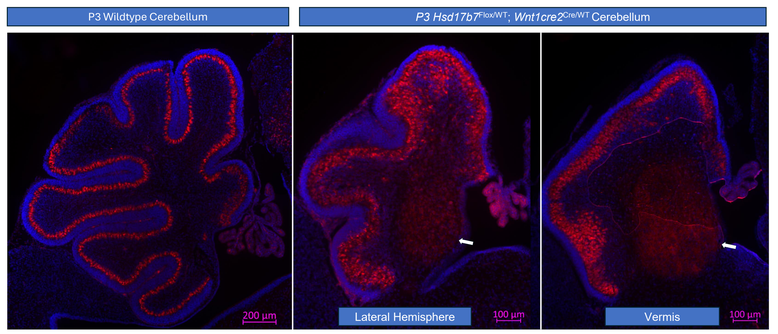

Calbindin IHC: *Hsd17b7*$^{Flox/WT}$; *Wnt1cre2*$^{Cre/WT}$ cerebella feature thickened bands and clumping of Purkinje cells with vastly increased signaling from the region of the deep cerebellar nuclei (arrow). A cell count on NIS-elements of red channel cells within folia revealed no significant difference between cell counts between wildtype and *Hsd17b7*$^{Flox/WT}$; *Wnt1cre2*$^{Cre/WT}$.

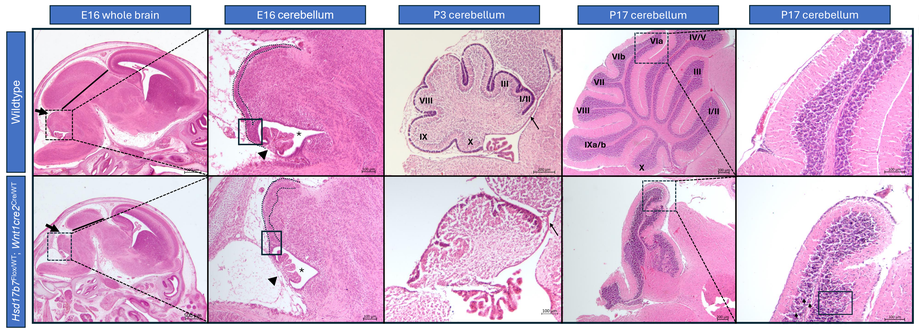

Cerebellar histology: At timepoint E16.5 the cerebellar hemisphere of the *Hsd17b7*$^{Flox/WT}$; *Wnt1cre2*$^{Cre/WT}$ mouse (dashed box) is small with an incompletely folded choroid plexus (arrowhead), a misshaped 4th ventricle (asterisks), a dysplastic paucicellular upper rhombic lip (solid square), and an unorganized superficial stratum (dotted line). It has a truncated lateral wall of the midbrain (solid line) and increased space between the mesencephalon and cerebellar hemisphere (arrow). At P3, the cerebellum is hypoplastic and there is severe loss of folia. The isthmic roof plate (arrow on control) is truncated. By P17, the cerebellum is extremely dysplastic and too distorted to determine normal landmarks. Closer examination of individual folia (dashed square) reveals clumping (solid square) and incomplete migration (arrows) of Purkinje cells.

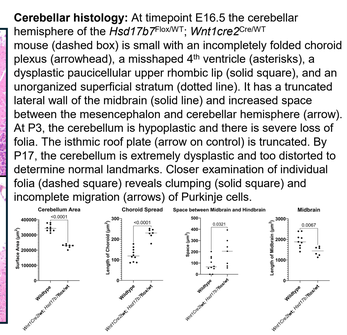

Conclusions/Discussion

- Our data reveals that loss of *Hsd17b7* in *Wnt1* cell lineages **does** lead to developmental abnormalities within structures arising from the midbrain hindbrain boundary.

Proposed Mechanisms; Congenital hydrocephalus

- While the formation of the SCO is not fully understood, past research has shown that *Wnt1* lineages are vital to the formation of the posterior SCO[5]. We proposed that **in the absence of *Hsd17b7, Wnt1* cell lineages are non-viable, leading to disrupted SCO formation. This causes impeded cerebral spinal fluid flow and secondary hydrocephalus.**

Proposed Mechanisms; Cerebellar changes

E11.5 mouse rhombencephalon depiction; Sagittal plane | E11.5 mouse rhombencephalon depiction; Transverse plane | E11.5 mouse cerebellar primordia; Sagittal plane

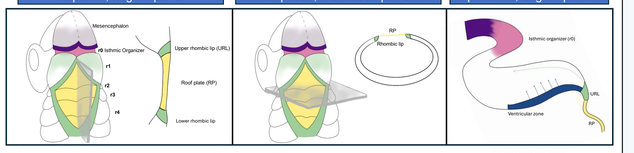

- Before E8.5, *Otx2* (cloudy purple) and Gbx2 (cloudy green) overlap to determine the midbrain-hindbrain boundary. At E8.5, *Fgf8* and *Wnt1* expression are activated at the interface[6].
- *Fgf8* (pink) defines R0, the isthmic organizer, and drives neurogenesis of the cerebellar primordia, while *Wnt1* (dark purple) marks the edge of the mesencephalon and drives neurogenesis of the mesencephalon[6].
- Cell to cell signaling between *Fgf8* and *Wnt1* is required at the isthmus for proper neurogenesis of both regions.
- At E9, the neural tube closes and the alar plate of r1 gives rise to the roof plate dorsally (yellow, becomes choroid plexus epithelium of the 4th ventricle), the ventricular zone (blue, gives rise to Purkinje cells and unipolar brush cells), and the rhombic lip dorsally (light green, gives rise to granular cell precursors)[6].
- **Microscopic changes noted at the rhombic lip and roof plate as well as migration of Purkinje cells in the face of correct anatomic positioning of the rhombencephalon suggests that the ischemic organizer is disrupted after the point of Otx2-Gbx2 patterning.**

Depiction of cerebellar region establishment in mice over time in the context of URL granular cells (modeled from Sgaier et al.)

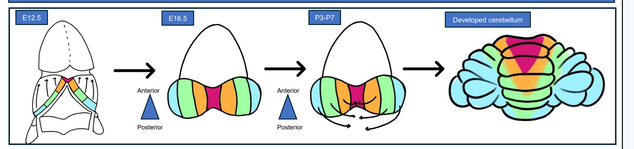

- During cerebellar development, the rostral-caudal axis of dorsal r1 undergoes a 90° rotation to become the medial-lateral axis at P3[6,7]. The lateral aspects move in more caudally than the medial aspect moves rostrally, leading to a V-shaped formation[6,7]. During this process, the vermis remains closest to the isthmic organizer and is more influenced by Fgf8 signaling more than the lateral hemispheres[6,7].
- **The vermes has a more severe phenotype than the lateral hemispheres which further supports pathology at the level of the isthmic organizer.**
- Based on previous literature and the presented findings, we propose that ***Hsd17b7* vital for the survival of the isthmic organizer and, in turn, proper neurogenesis of the cerebellum.**

Implications and Relevance

- Our model shows that *Hsd17b7* and proper cholesterol biosynthesis are required for dorsal midline development and midbrain-hindbrain boundary patterning.
- Based on our findings, we suspect that without *Hsd17b7, Wnt1* cell lineages die, leading to loss of the isthmic organizer and the subcommissural organ.
- Hydrocephalus and cerebellar hypoplasia have been rarely linked with some, though not all, cholesterol biosynthesis malformation syndromes. The presence of this rare phenotype within this model offers an opportunity to explore the differences between cholesterol biosynthesis malformation syndromes that feature hydrocephalus and cerebellar phenotypes and those that do not. This may lend credence to the theory of toxic precursors as a main driver of disease.

Next Steps

Immediate

- **Elucidate the mechanisms behind the cerebellar phenotype.** With a specific direction in mind (disruption of the isthmic organizer after E8.5), we can select more in-depth experiments in which to complete our second objective. Planned experiments include:
  - Whole mount imaging of *Hsd17b7*$^{Flox/WT}$; *Wnt1cre2*$^{Cre/WT}$ mice with a fluorescent protein at timepoints E9, E10, and E12.5 to better understand how loss of *Hsd17b7* impacts the isthmic organizer and downstream differentiation of cerebellar primordia
- **Explore phenotypes outside of the brain.** Outside of changes in the brain, we have also found that this mouse model sometimes has a cleft palate of varying severity. Similar *Wnt1cre2* models have also been associated with pathologic changes of ganglia and the heart.
  Planned experiments include:
  - H&E and skeletal preps of the cleft palate phenotype
  - Possible H&E of enteric organs, gross heart dissections
- **Tissue specific ablation of *Hsd17b7* from the forebrain.** Our past research with the "*Rudolph*" hypomorph illustrates pathologic changes within the forebrain. We are currently running similar tissue specific ablation experiments on an *Emx1-cre* background to explicate the underlying mechanisms.

Long term

- The overarching goals of this research are threefold: to **understand the mechanisms** behind disease within the cholesterol biosynthesis pathway; to **discover the role of toxic cholesterol precursors** within the unique expression of disease at different points within the cholesterol biosynthesis pathway; to leverage a better understanding of these complex mechanisms and molecular interplay to **identify more effective therapeutic targets**

Acknowledgements and Funding

Special thanks to the members of the Stottmann lab for their keen input and guidance, the veterinary team at NCH for their dedication to the health and wellness of this mouse colony, and Andrew Vontell for the initial breeding and maintenance of this mouse line. Funding is supported by the Ohio State University Graduate School and Abigail Wexner Research Institute. The authors state no conflicts of interest.

Citations

1. Cerqueira, N., Oliveira, EF., Gesto, DS., Santos-Martins, D., Moreira, C., Moorthy, HN., Moorthy, HN., Ramos, MJ., & Fernandes, PA. (2016). Cholesterol biosynthesis: A mechanistic overview. *Biochemistry,*55(39),5483–5506.
2. Marijanovic, Z., Laubner, D., Möller, G., Gege, C., Husen, B., Adamski, J., & Breitling, R. (2003). Closing the gap: Identification of human 3-ketosteroid reductase, the last unknown enzyme of mammalian cholesterol biosynthesis. *Molecular Endocrinology,17*(9),1715-1725.
3. Stottmann RW., Turbe-Doan A., Tran P., Kratz LE., Moran JL., Kelley RI., & Beier DR.(2011) Cholesterol metabolism is required for intracellular hedgehog signal transduction in vivo. *PLoS Genetics,7*(9):e1002224.
4. Driver AM, Kratz LE, Kelley RI, & Stottmann RW. (2016). Altered cholesterol biosynthesis causes precocious neurogenesis in the developing mouse forebrain. *Neurobiology of disease,91*(1):69-82.
5. Dietrich, P., Shanmugasundaram, R., E, S., & Dragatsis, I. (2008). Congenital hydrocephalus associated with abnormal subcommissural organ in mice lacking huntingtin in Wnt1 cell lineages. *Human molecular genetics 18*(1):142-150.
6. Manto, MU., Gruol, DL., Schmahmann JD., Koibuchi, N., & Sillitoe, RV. (Eds.) (2022). *Handbook of the cerebellum and cerebellar disorders* (2nd ed.).
7. Springer Sgaier, SK., Lao, Z., Villanueva, MP., Berenshteyn, R., Stephen, D., Turnbull, RK., Joyner., AL. (2010). Genetic subdivision of the tectum and cerebellum into functionally related regions based on differential sensitivity to engrailed proteins. *Development, 134*(12):2325-2335.

Development of an HTLV-1 mRNA vaccine using a NZW rabbit model

Emily King[1], Joshua Tu[1], Victoria Maksimova[1], Susan Smith[1], Ramon Macias[1], Xiaogang Cheng[2], Tanmayee Vegesna[3], Lianbo Yu[1], Lee Ratner[2], Patrick Green[1], Stefan Niewiesk[1], Justin Richner[3], Amanda Panfil[1]

[1]The Ohio State University, Columbus, OH 43210, USA, [2]Washington University in St. Louis, St. Louis, MO 63130 USA, [3]University of Illinois Chicago, Chicago, IL 60607 USA

THE OHIO STATE UNIVERSITY
COLLEGE OF VETERINARY MEDICINE

Human T-cell leukemia virus type 1:

- Human T-cell leukemia virus type 1 (HTLV-1) is an oncogenic human retrovirus
- HTLV-1 causes adult T-cell leukemia/lymphoma (ATLL) and HTLV-1 associated myelopathy/tropical spastic paraparesis (HAM/TSP)
- Disease is driven by the clonal expansion of HTLV-1-infected CD4$^+$ T-cells
- Viral accessory genes (*Tax*, *Hbz*) play a key role in viral persistence and pathogenesis

Background:

The challenges of making an HTLV-1 vaccine:

- Viral integration
- HTLV-1 transmission exclusively cell-to-cell
- Envelope (Env; gp62) structure has not been resolved

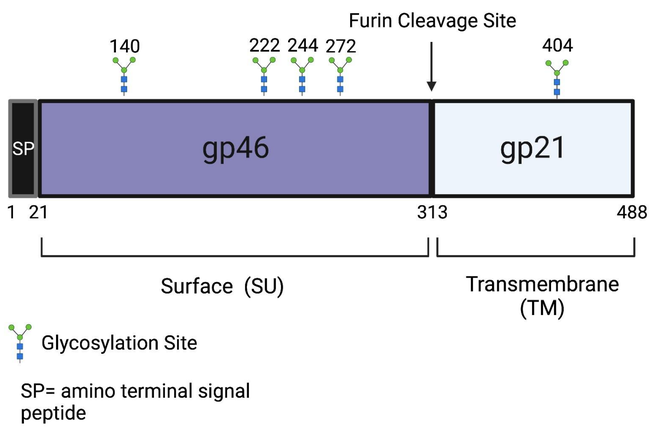

Figure 1. Schematic of the HTLV-1 Env (gp62) glycoprotein. Env is comprised of two subunits (gp46 and gp21), which are cleaved at a furin cleavage site. Glycosylation sites are denoted.

The feasibility of making an HTLV-1 vaccine:

- Less sequence diversity (compared to HIV-1)
- Several well-established animal models to study early infection and disease
- Env has few glycosylation sites (5 vs 25 in HIV-1)
- Env elicits both humoral and cellular immune responses in infected individuals

HTLV-1 infection of rabbits mimics early infection in humans:

- Rabbits inoculated with HTLV-1 become persistently infected
- Early rabbit humoral antibody responses against Gag and Env mimic asymptomatic early viral infection in humans
- Animals do not develop disease, but do recapitulate viral persistence (i.e., long-term viral latency)

Scientific Premise:

We **hypothesize** an envelope mRNA-LNP vaccine will protect against HTLV-1 infection.

Results:

In vitro characterization of the codon optimized HTLV-1 envelope construct

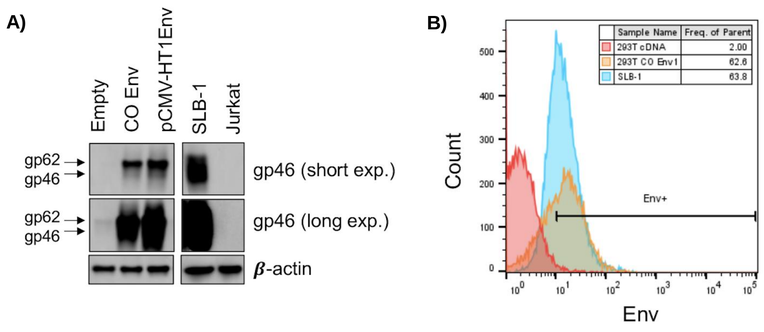

Figure 2. Empty vector (cDNA), codon optimized envelope (CO Env), or pCMV-HT1Env plasmid were transfected into HEK293T cells. (A) Protein expression was evaluated by western blot using gp46 antibody or β-actin (loading control). SLB-1 cells were included as a positive control and Jurkat cells served as a negative control. (B) Cell surface expression of envelope was measured by flow cytometry. SLB-1 cells (blue peak) were included as a positive control for surface expression of envelope protein.

Results:

Env mRNA-LNP is immunogenic and decreases proviral load in New Zealand rabbits

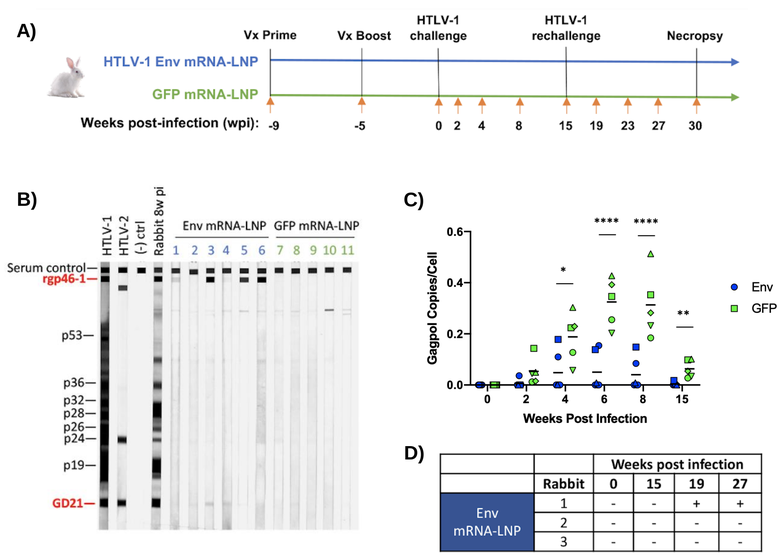

Figure 3. (A) Study timeline. New Zealand white rabbits were vaccinated with two doses of Env mRNA-LNP (n=6) or a control GFP mRNA-LNP (n=5). Rabbits were challenged with lethally irradiated HTLV-1 producer cells at two separate time points designated 0- and 15-weeks post-infection (wpi). Peripheral blood was collected at weekly time points, as indicated by red arrows. Rabbits were necropsied 30 weeks after viral challenge. (B) The HTLV-1 antibody response was qualitatively assessed 4 weeks after vaccine prime and boost using a modified MP Diagnostics HTLV Blot 2.4 Western Blot Assay. (C) 1 x 10^7 lethally irradiated HTLV-1 producer cells were inoculated into NZW rabbits via the lateral ear vein at week 0 (5 weeks post vaccination) and week 15 (20 weeks post vaccination). Whole blood was collected at Week 0 (pre-inoculation) and Weeks 2, 4, 6, 8, 15, 19, and 27 post-infection (study endpoint) for plasma and rPBMC isolation. Genomic DNA was isolated from rPBMCs and proviral load was measured by qPCR using a primer and probe set specific to HTLV-1 gag/pol sequence. Each symbol represents an individual rabbit. Linear mixed model was used for statistical analysis. Tukey's method was used for adjusted p-value. *P ≤ 0.05, **P ≤ 0.01, ****P ≤ 0.0001. (D) Tax-based nested PCR was performed with genomic DNA collected at weeks 0, 15, 19, and 27 post-infection. A positive (+) or (-) symbol is reported for the detection of proviral DNA for each rabbit.

Env mRNA-LNP vaccine decreases viral gene expression *in vivo*

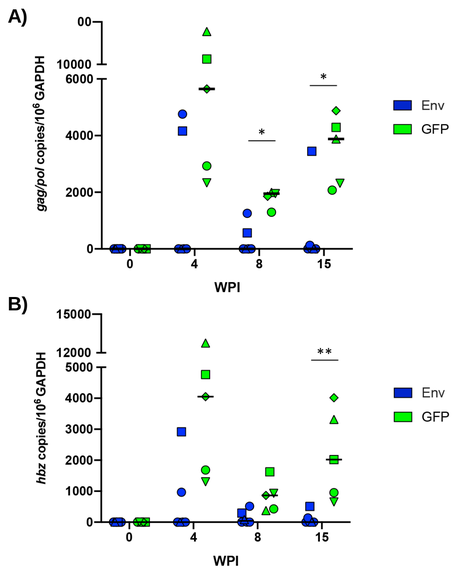

Figure 4. RNA was isolated from rPBMCs for cDNA synthesis. cDNA was subjected to 12-cycle pre-amplification reactions and pre-amplified products were diluted for downstream qPCR to detect viral gene expression. Copy numbers of *gag/pol* (A) and *hbz* (B) are shown relative to 1 x 10^6 *rgapdh* copies. In each of the graphs, symbols represent the gene expression for a single inoculated rabbit and bars represent the mean. Linear mixed-effects analyses were performed, and Tukey's method was used for adjusted p-value. *P ≤ 0.05, **P ≤ 0.01.

Intracellular IFN-γ production in CD4 and CD8 T cells in response to Env mRNA-LNP vaccination

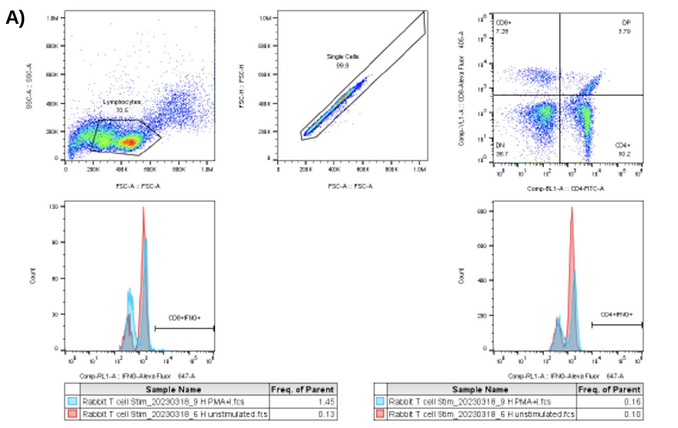

Figure 5. Rabbit PBMCs were cultured *ex vivo* with PMA/Ionomycin (PMA/I), RSV peptide (negative control), or various Env peptide pools. After overnight stimulation, cells were fixed, permeabilized, stained, and analyzed by flow cytometry for CD4, CD8, and IFN-γ expression. (A) Flow gating strategies used to identify CD4+IFN-γ+ and CD8+IFN-γ+ populations in stimulated healthy rabbit PBMCs. Percentage of IFN-γ+ cells in the CD4$^+$ (B) and CD8$^+$ T-cell populations (C) in Env and GFP mRNA-LNP vaccinated rabbits after vaccination (week 0) and 2 weeks after viral infection were pooled. (B-C) Each symbol represents an individual rabbit.

Results:

Env mRNA-LNP vaccine elicits neutralizing antibody responses

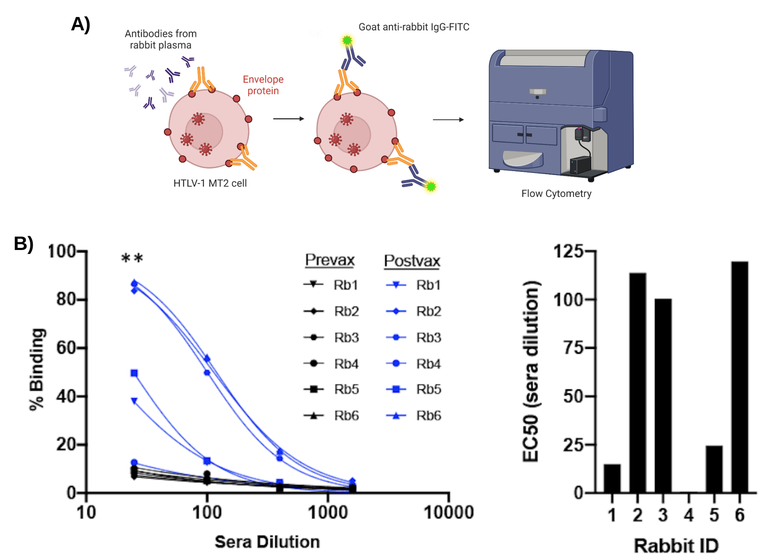

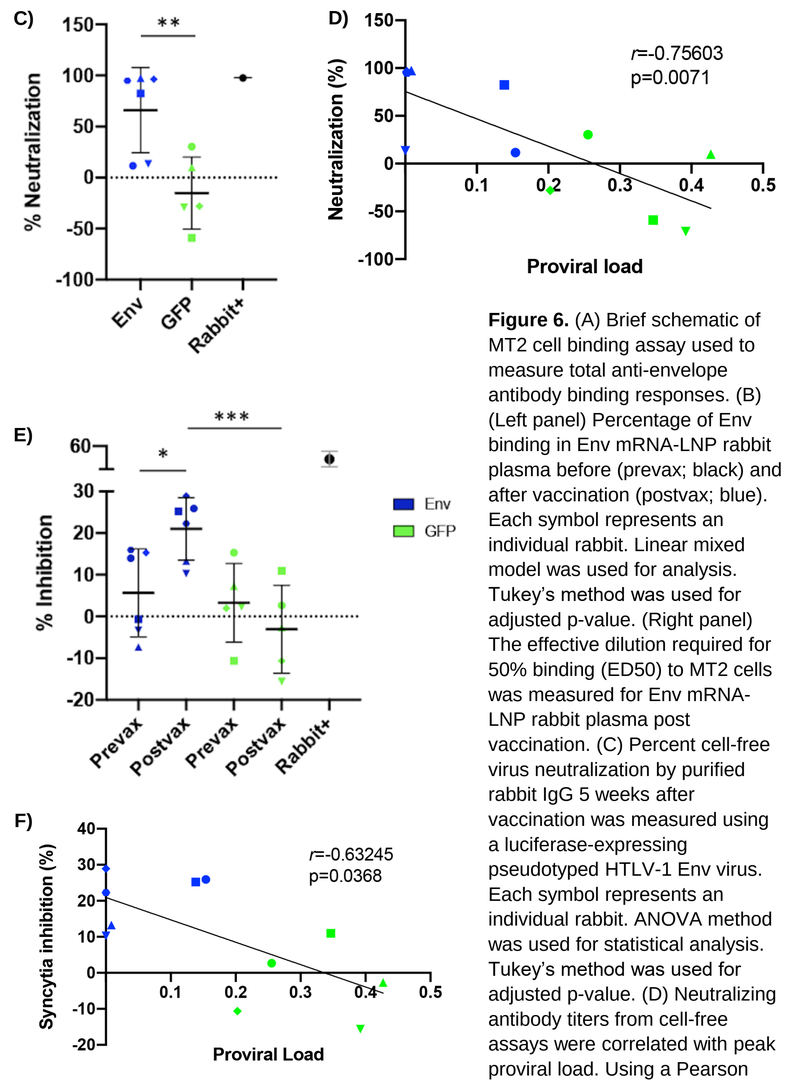

Figure 6. (A) Brief schematic of MT2 cell binding assay used to measure total anti-envelope antibody binding responses. (B) (Left panel) Percentage of Env binding in Env mRNA-LNP rabbit plasma before (prevax; black) and after vaccination (postvax; blue). Each symbol represents an individual rabbit. Linear mixed model was used for analysis. Tukey's method was used for adjusted p-value. (Right panel) The effective dilution required for 50% binding (ED50) to MT2 cells was measured for Env mRNA-LNP rabbit plasma post vaccination. (C) Percent cell-free virus neutralization by purified rabbit IgG 5 weeks after vaccination was measured using a luciferase-expressing pseudotyped HTLV-1 Env virus. Each symbol represents an individual rabbit. ANOVA method was used for statistical analysis. Tukey's method was used for adjusted p-value. (D) Neutralizing antibody titers from cell-free assays were correlated with peak proviral load. Using a Pearson correlation coefficient, we found neutralizing Ab activity was negatively correlated with proviral load at 6 wpi. (E) Neutralizing Ab activity was measured using a syncytia inhibition assay. Percent inhibition was calculated by taking the average number of syncytia counted in rabbit sera wells divided by the average number of syncytia in virus control wells (no sera), multiplied by 100. Sera samples prior to vaccination (prevax) and 5 weeks after vaccine boost (postvax) were measured. Each symbol represents an individual rabbit. Linear mixed model was used for analysis. Tukey's method was used for adjusted p-value. Rabbit+; Sera from a rabbit infected with HTLV-1. (F) Neutralizing antibody activity from syncytia inhibition assays was correlated with peak proviral load. Using a Pearson correlation coefficient, we found neutralizing Ab activity was negatively correlated with proviral load at 6 wpi.

Conclusions:

Env mRNA-LNP vaccine can protect against cell-associated viral challenge

- Sterilizing immunity against primary challenge in 3/6 Env mRNA-LNP vaccinated rabbits and against rechallenge in 2/3 rabbits
- Decreased proviral load and gene expression in Env mRNA-LNP vaccinated rabbits

Env mRNA-LNP is immunogenic

- Primes the cellular response, increasing CD4+IFN-γ+ and CD8+IFN-γ+ populations 2 weeks post infection
- Elicits neutralizing antibody responses that are negatively correlated with proviral load (immune correlate of protection)

Funding:

This work was supported by a NIH National Cancer Institute Program Project Grant (P01CA100730), The Ohio State University Pelotonia Fellowship Program, a seed grant from The Ohio State University Comprehensive Cancer Center Leukemia Research Program, and a seed grant from the Washington University Center for Drug Discovery.